2025,Volume 2 , Issue 7 , PSIJK (46-52)

Pure Sciences International Journal of Kerbala

Synthesis and Characterization of Indium Phosphide by Electrochemical Deposition Method

Imad Kadhim Khudhair [a*]

[a] Ministry of Education, Baghdad Education Directorate of Al- Karkh , Iraq

P A P A R I N F O

Received: 11.05.2025
Accepted: 22.06.2025
Published: 30.09.2025

Keywords:
Indium phosphide, Electrochemical deposition method, X-ray diffraction, Electrical properties, thermoelectric properties.

A B S T R A C T

Three samples of indium phosphide (InP) were prepared by electrochemical deposition method on porous nickel substrates. The results of X-ray diffraction of InP showed that it crystallizes in one direction (220). There is an increase in the intensity of the diffraction peak with increasing deposition time for the prepared samples. By calculating (C-V) at a fixed frequency and drawing the relationship between the (1/C2) and (V), it was found that the slope has a negative value, indicating that the prepared samples are of the p-type, the built-in potential (Vbi) of the samples was determined to be (1.42, 1.54, 1.66)eV.(I-V) was calculated for the samples prepared for InP at different temperatures (303,313,323)ko , the relationship between I and V showed that the current intensity increases with increasing temperatures, and the electrical resistance (R) of the samples decreases with increasing different temperatures, the activation energy (Ea) values of the samples ranged (0.14,0.07,0.06) eV at different temperatures. from the study of the thermoelectric properties, it was found that the best value of the Seebeck coefficient (S) is for the sample with a deposition time of (4h).

DOI: 10.53851/psijk.v2.i7. 46-52

Table 1. Nomenclature and Definitions Used in the Study

InP	Indium phosphide	ε	crystal lattice strain
XRD	X-ray diffraction	δ	dislocation density
FCC	Face centered cubic	Ψ	barrier height of the system
WZ	Wurtzite	V_{bi}	built-in potential
ZB	zincblende	R	electrical resistance
aδ	crystal lattice constant	Ea	activation energy
nm	nanometer	K	Boltzmann constant
d_{hkl}	distance between the crystal planes	S	Seebeck coefficient
N	integer called diffraction order	FWHM	Full Width at Half Maximum
D	crystallite size		

*Corresponding Author Institutional Email:
emadkadhem20@gmail.com (Imad Kadhim Khudhair)

1.INTRODUCTION

Nanostructured semiconductors have attracted much attention due to their good optical properties, especially nanowires belonging to group (III-V) which are well-known electronic and optoelectronic materials (Li, He, et al., 2023) , and can cover important spectral ranges extending from the visible to the infrared range. The direct energy gap is one of the main advantages of most compound semiconductors of group (III-V) (Cipriano, Di Liberto, et al., 2020), making the study of these materials very desirable. Among these compounds is indium phosphide (InP) (Li & Lu, 2008). Indium phosphide has a direct energy gap (1.42-1.35) eV, at 300K^{o} and has an absorption wavelength between (873-918) nm (Al Hammade, 2022) , in the infrared range (Almeida, Ubbink, et al., 2023) , and has various applications in electronics and optoelectronic devices as it is characterized by high electronic mobility (4000 cm^2/V.S) (Yue, Shi, et al., 2023). The crystal structure of indium phosphide is face-centered cubic (FCC). It exists in two crystal forms (WZ), (ZB) as in Figure (1), and its crystal lattice constant is (a= 5.8687A^{o}).Its molar mass is (145.792 g/mol) and its density is (4.81g/cm^3).

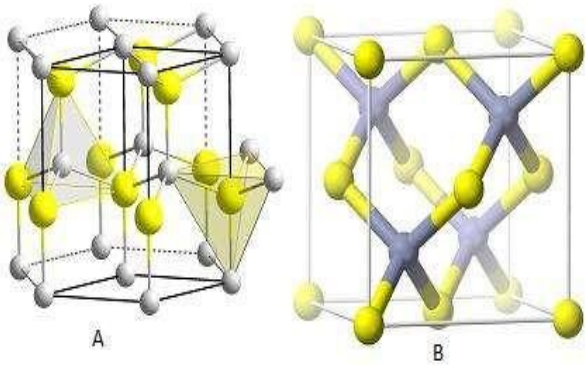

Figure 1. Shows the crystal structure of (InP),(A) Wurtzite and (B) zincblende (Almeida, Ubbink, et al., 2023)

Applications of indium phosphide include solar cells (Lasheer, Fathy, et al., 2023), photodiodes, photosensitive sensors, light-emitting diodes (LEDs) (Sticklus, Hoeher, et al., 2020), transistors (FETS) (Malik & Kharadi, 2020), wireless communications, medical and biological applications (Almeida, Ubbink, et al., 2023) (Bhagya & Kim, 2021) .InP nanowires can be fabricated using several techniques including multiphase (vapor-solid-liquid) method (Jafari Jam, Persson, et al., 2020) , organic complex method (Zhang, Xu, et al., 2017) solution-phase (liquid-solid) method, hot solution method (Wang, Dong, et al., 2016) .laser-assisted growth method (Ahmed, Qi, et al., 2023) , and electrochemical deposition method (Zhang, Feng, et al., 2020). This is the method used in this research. The electrochemical method is a simple and inexpensive method compared to other preparation methods. Many parameters (concentration, temperature, deposition time) can be changed, which ultimately affect the properties of the prepared compound.

2. THEORETICAL CONSIDERATIONS

Based on Bragg's law for X-ray diffraction in relation (1), we can determine the distance between the crystal planes (d_{hkl}). $2d_{hkl}\ Sin(\Theta_{hkl}) = n\lambda$ ……(1)

Where θ= diffraction angle, n= integer called diffraction order, λ= wavelength of X-rays (λ=1.5405A˚). The crystal lattice constant was calculated using the relation (2) which gives the crystal distance of the parallel planes in terms of the crystal lattice constants of the face-centered cubic structure: (Bandoh, Nkrumah, et al., 2021) (Bandoh, Nkrumah, et al., 2021)

$a = d\sqrt{h^2 + k^2 + l^2}$ ……(2),

where a (crystal lattice constant). From the Scherrer equation, the crystallite size (D) was calculated

$$D = \frac{k\lambda}{\beta cos\theta} \text{ ……(3),}$$

where k= constant (0.9), β =Full Width at Half Maximum (FWHM) of the diffraction peak, θ= diffraction angle, λ= wavelength of X-rays (Ravi & Chitra, 2020). The crystal lattice strain (ε) and the dislocation density (δ) in the crystal lattice were calculated using the two relationships. (Filipovic, Obradovic, et al., 2018),

$$\varepsilon = \frac{\beta Cos\theta}{4} \text{ …….(4) ,}$$

$$\delta = \frac{n}{D^2} \text{ ……..(5), where (n=1).}$$

The type of semiconductor can be determined from the Schottky relationship. (Ashajyothi & Reddy, 2021) , $\left(\frac{1}{C} - \frac{1}{2C_0}\right)^2 = \frac{2}{e\,\epsilon_o \cdot \epsilon_r\,(N_d - N_a)}(\psi + V)$ ……(6), where (e) electron or elementary charge, (ε_r) relative permittivity, (ε_o) permittivity of free space, (N_d) density of donor atoms, (N_a) density of acceptor atoms , (Ψ) barrier height of the system. (C_o), (C) are the capacitance per unit area of a grain boundary biased and (V) volts. We find from the relationship (6) that when the density of the acceptor atoms is greater than the density of the donor atoms, (N_a>> N_d). the density of donor atoms can be neglected, and therefore when plotting the changes in ($1/C^2$) in terms of the applied voltage (V) on the prepared samples, we obtain a graph with a negative slope. This means that the semiconductor is of the p-type, and if (N_d>> N_a) then when plotting the changes in ($1/C^2$) in terms of (V), we get a

graph with a positive slope, so the semiconductor is of the N-type

The activation energy (Ea) was calculated based on the following relationship:

$I = I_o\, e^{-Ea/kT}$……(7) (Filipovic, Obradovic, et al., 2018) (Schubert, 2022) where I= current intensity at temperature (T), I_o = current intensity at absolute zero, k= Boltzmann constant. Taking the (lnI) of relation (7) we get

$\ln I = \ln I_o - Ea/kT$ ……..(8).

The Seebeck coefficient (S) (which is the basis for choosing the material in power generation devices) was found for the samples prepared using the electrical circuit shown in figure (2) within the range of temperature changes of (310-430) k^o through the following equation.

$S = \frac{\Delta V}{\Delta T}$ ……..(9) (Van & Mitterhuber, 2023) .

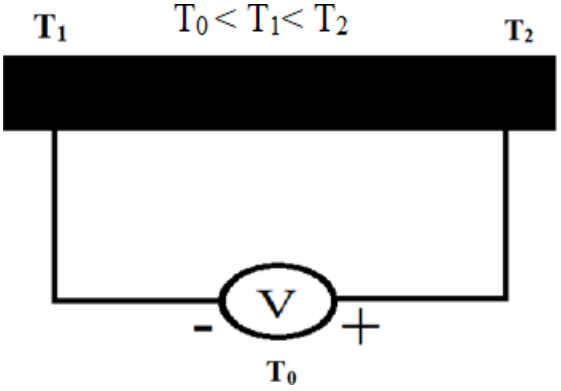

Figure 2. Electrical circuit (Seebeck coefficient)

3. EXPERIMENTAL PART

A high purity nickel substrate was taken and its surface was smoothed with sandpaper of different sizes to obtain a mirror-smooth surface. The substrate was cleaned with a solution of (CH_3COOH) and (CH_3COCH_3) using an ultrasonic device to enhance the surface quality of the substrate, after which the surface was oxidized under a constant voltage of (40)V at (0.3)mol/L of oxyacetylene as an electrolyte for 30min. The substrate was used as anode and the temperature was maintained at 25°C during oxidation. After that, the oxide layer was etched with 0.5% of HCL at a temperature of 65°C for 20minutes. Thus, a large number of surface pores were obtained in the Ni substrate, which is suitable for Indium phosphide (InP) deposition. After that, the oxide layer was removed from the back part of the slide and attached with an insulating tape to prevent the deposition of (InP) on the back part, but the deposition was only on the front part that contains the surface pores.

Indium chloride ($InCl_3$) solution was prepared by dissolving (0.482)gm in indium oxide (In_2O_3) in 50 ml of distilled water and placing it on a magnet, then add a few drops of (HCl) until complete dissolutionm, after that a solution of indium chloride ($InCl_3$) and phosphorus acid (H_3PO_4) was prepared.

The surface-porous nickel substrate were washed with ethanol and then washed with distilled water. A nickel substrate was used as a cathode and a platinum electrode was used as an anode. They were placed in the prepared electrolyte solution where the distance between the two electrodes was (3cm) under a voltage (5)V. The deposition process continued for two hours for the first substrate, denoted as (2h), three hours of deposition for the second substrate denoted as (3h), and four hours of deposition for the third substrate denoted as (4h). The samples were washed several times with distilled water and placed under a temperature of 200 ^{o}C for two hours. Thus three samples of InP were obtained

4. RESULTS AND DISCUSSION

Figure (3) shows the X-ray diffraction of the prepared (InP) samples. The crystal planes formed follow the cubic structure and they are face centered cubic (FCC), with the appearance of three peaks for nickel and one peak for (InP) in the direction (220). This indicates that InP crystallizes in one direction when

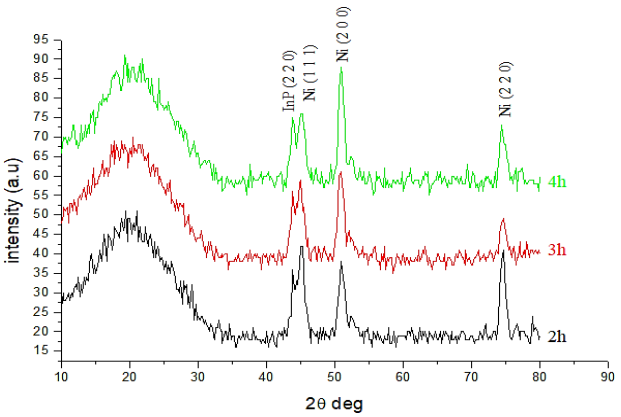

Figure 3. X-ray diffraction of prepared InP samples.

growing on a nickel substrate with surface pores. It is also clear that the intensity of the diffraction peak increases with increasing deposition time. This means that the

growth of the samples increases with deposition time. Based on Bragg's law for X-ray diffraction in relation (1), we can determine the distance between the crystal planes (d_{hkl}). The crystal lattice constant was calculated using the relation (2) which gives the crystal distance of the parallel planes in terms of the crystal lattice constants of the face-centered cubic structure. From the Scherrer equation, the crystallite size (D) was calculated using the relation (3). The crystal lattice strain (ε) and the dislocation density (δ) in the crystal lattice were calculated using the two relationships. (4), (5). The table (2) reveals the values of the distance between crystal planes, crystal lattice constanat, crystallite size, crystal lattice strain and dislocation density for InP wires prepared on nickel substrates with surface pores in the (220) direction where there is an increase in the values of (ε) and (δ) and a decrease in the values of (D).This indicates the presence of crystal distortion

Table 2. Shows the results of X-ray diffraction of the prepared InP wires.

	2θ	d(A^0)	a(A^0)	β (rad)	D (nm)	$\varepsilon \times 10^{-4}$ (lines^{-2}.m^{-4})	$\delta \times 10^{14}$ (lines/m^2)
2h	43.8	2.065	5.83	0.0034	45.90	7.88	4.74
3h	43.8	2.065	5.83	0.0061	25.58	14.14	15.28
4h	43.8	2.065	5.83	0.0087	17.93	20.18	31.10

To determine the type of semiconductor, the capacitance was measured with a device (LCR- meter) with a variable voltage (0.1-2)V at a fixed frequency (1KHZ) at room temperature. From the relationship between ($1/C^2$) and (V) for the prepared samples, the graphs shown in figure (4) showed linear relationships with negative slopes. This indicates that the semiconductor formed is of the p-type. Even at voltage (0.5)V the slope is negative and at values greater than (0.5)V the slope is also negative. Thus, the total slope is negative. As shown in the figure (4) there is a large decrease in capacitance at (0.22)V and a small decrease in capacitance that is almost constant when the voltage increases to (2)V.

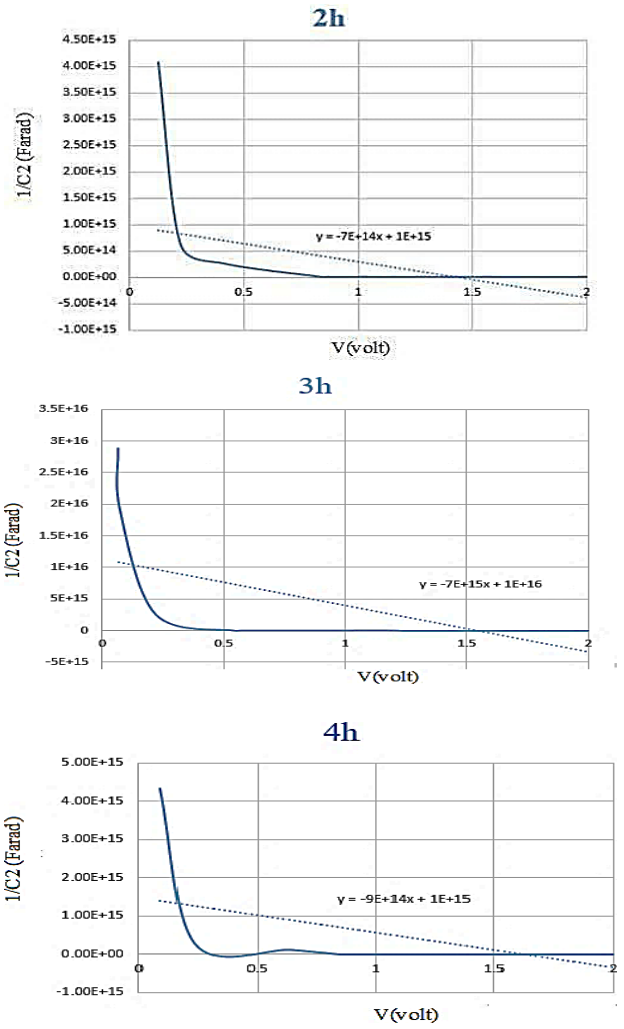

Figure 4. Variations of ($1/C^2$) with respect to (V) for prepared samples

Figure (4), we find the built-in potential (V_{bi}) of the samples prepared from the point of intersection of the slope line with the V-axis, we notice that increases the deposition time of the prepared samples increases the values of (V_{bi}) as shown in table (3)

Table 3. V_{bi} values for prepared samples.

Deposition time	2h	3h	4h
V_{bi} (eV)	1.42	1.54	1.66

To identify the electrical properties of the prepared samples of (InP), the (I-V) characteristics were studied at different temperatures (303, 313, 323) k^o As shown in figure (5), the relationship between current and voltage is a linear relationship, and the current intensity increases with increasing temperature, which in turn increases the

movement of charge carriers, leading to an increase in electrical conductivity.

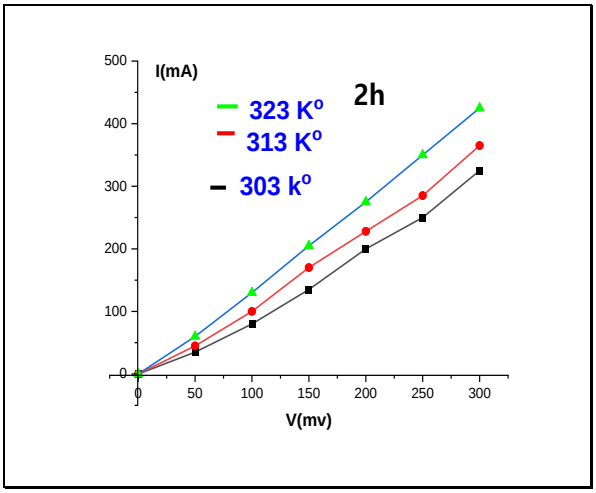

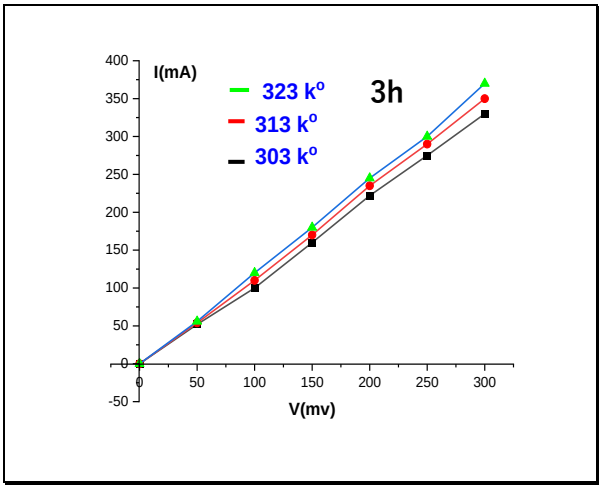

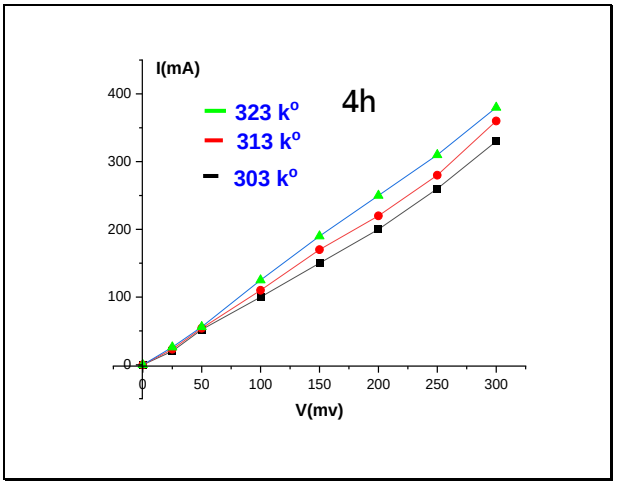

Figure 5. (I-V) For samples prepared InP at different temperatures.

By studying changes in electrical resistance with temperature changes of (303, 313, 323) k° for the samples prepared at (300)mV, and as they are shown in figure (6)

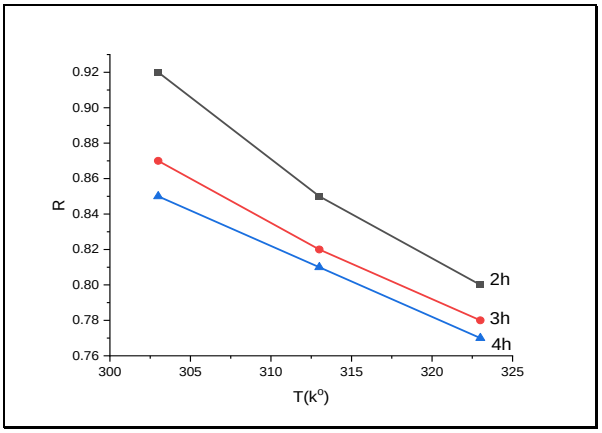

Figure 6. Shows the decrease in electrical resistance (R) of InP with increasing temperatures.

The data exhibits an approximately linear relationship. This is due to the increase in the movement and density of charge carriers thermally, which indicates that the behavior of InP is a natural behavior for semiconductors, as the electrical resistance of the prepared samples decreases with increasing temperatures according to table (4).

Table 4. Showing the decrease in electrical resistance of InP samples with increasing temperatures

	2h	**3h**	**4h**
T(k⁰)	**R(Ω)**	**R(Ω)**	**R (Ω)**
303	0.92	0.87	0.85
313	0.85	0.82	0.80
323	0.80	0.78	0.77

The relationship between (lnI) and (1/T) is shown in the figure (7).

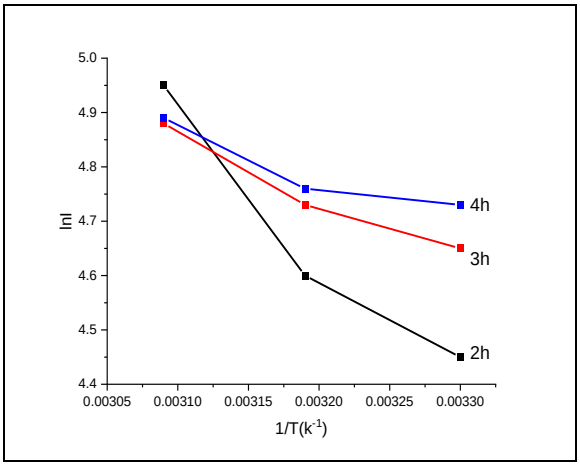

Figure 7. Shows the changes in (lnI) as a function of (1/T) for InP.

From the slope of the straight line in the curves resulting from figure (7) and by applying the relationships (7),(8) the (E_a) values for InP were calculated at temperatures of (303, 313, 323) k^o as shown in table (5).

Table 5. Shows the (E_a) values of InP.

Depositin time	E_a(eV)
2h	0.14
3h	0.07
4h	0.06

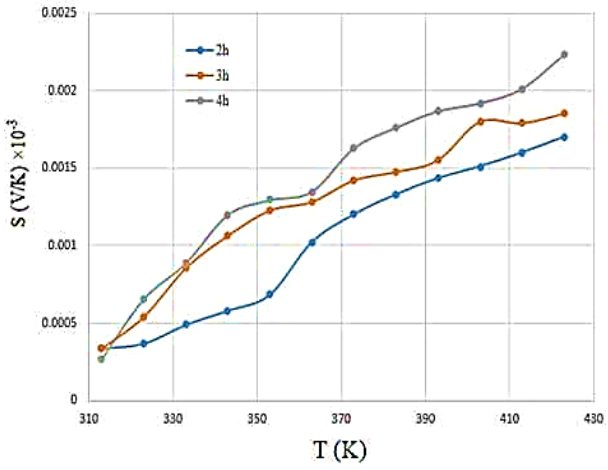

Figure 8. Shows the changes in (S) as afunction of temperature changes for InP.

Using relation (9) the Seebeck coefficient (S) was found. Figure (8) shows that (S) has a positive value. This confirms that the formed semiconductor is of the p-type. The best value of (S) for the sample is InP at a deposition time of (4h).

5. CONCLUSION

The results of X-ray diffraction of InP showed that it crystallizes in one direction (220), and increase in the intensity of the diffraction peak with increasing deposition time for the prepared samples. It was found from the calculation of (C-V) that the slope is negative value. This indicates that the prepared samples are of the p-type. (V_{bi}) which was determined to be (1.42, 1.54, 1.66) eV. This increases the deposition time of the prepared samples and increases the values of (V_{bi}). (I-V) was calculated for the samples prepared for InP at different temp (303,313,323) k^o .The relationship between I and V showed that the current intensity increases with increasing temp, and electrical resistance (R) of the samples decreases with increasing different temp. (Ea) values of the samples ranged (0.14,0.07,0.06) eV at different temp. Seebeck coefficient (S) is positive for prepared samples. This confirms that the formed semiconductor is of the p-type. The best value of (S) for the sample is InP at a deposition time of (4h).

REFERENCES

Ahmed, N. M., Qi, L. X., et al. (2023). Investigating the Role of Temperature in Laser Assisted Chemical Bath Deposition for ZnO Growth for Photodetector Application. *Photonics*, *10*(8), 910. https://doi.org/10.3390/photonics10080910

Almeida, G., Ubbink, R. F., et al. (2023). InP colloidal quantum dots for visible and near-infrared photonics. *Nature Reviews Materials*, *8*, 742–758. https://doi.org/10.1038/s41578-023-00596-4

Ashajyothi, S., & Reddy, V. R. (2021). Influence of tin oxide (SnO2) interlayer on the electrical and reverse current conduction mechanism of Au/n−InP Schottky junction and its microstructural properties. *Thin Solid Films*, *740*, 139001. https://doi.org/10.1016/j.tsf.2021.139001

Bandoh, C. K., Nkrumah, I., et al. (2021). Effect of annealing on the structure and optical properties of lead selenide and cadmium selenide thin film

prepared by chemical bath deposition. *Chalcogenide Letters*, *18*(2), 81–89.

Bhagya, H., & Kim, E. B. (2021). Safe synthesis of InP quantum dots for Biological applications. *The Electrochemical Society*, *MA01*(23). https://doi.org/10.1149/MA2021-0123915mtgabs

Cipriano, L. A., Di Liberto, G., et al. (2020). Quantum confinement in group III-V semiconductor 2D nanostructures. *Nanoscale*, *12*, 17494–17501. https://doi.org/10.1039/D0NR03577G

Faroz A. Malik, G., & Kharadi, M. A. (2020). Performance analysis of indium phosphide channel based sub-10 nm double gate spin field effect transistor. *Physics Letters A*, *384*(19), 126498. https://doi.org/10.1016/j.physleta.2020.126498

Filipovic, S., Obradovic, N. N., et al. (2018). Physical properties of sintered alumina doped with different oxides. *Science of Sintering*, *50*(4), 409–419. https://doi.org/10.2298/SOS1804409F

Jafari Jam, R., Persson, A. R., et al. (2020). Template-assisted vapour–liquid–solid growth of InP nanowires on (001) InP and Si substrates. *Nanoscale*, *12*, 888–894. https://doi.org/10.1039/C9NR08025B

Lasheer, D., Fathy, M., et al. (2023). Synthesis and characterization of InP quantum dots for photovoltaics applications. *Journal of Materials Science*, *34*. https://doi.org/10.1007/s10854-023-10179-2

Li, G.-R., & Lu, X.-H. (2008). Electrochemical reduction synthesis of In–Sb nanoropes and terraced micropyramids. *Electrochemistry Communications*, *10*(1), 127–130. https://doi.org/10.1016/j.elecom.2007.11.007

Li, Z., He, Z., et al. (2023). Review on III–V Semiconductor Nanowire Array Infrared Photodetectors. *Advanced Materials Technologies*, *8*(13), 2202126. https://doi.org/10.1002/admt.202202126

Ravi, K., & Vchitra. (2020). Structural and Surface morphology of Lead Selenide (PbSe) thin films. *Materials Science and Engineering*, *932*, 012133. https://doi.org/10.1088/1757-899X/932/1/012133

Schubert, F. E. (2022). *Physical Foundations of Solid-State Devices* (e-book).

Sticklus, J., Hoeher, P. A., et al. (2020). Experimental Characterization of Single-Color Power LEDs Used as Photodetectors. *Sensors*, *20*(18), 5200. https://doi.org/10.3390/s20185200

T. B. Al Hammade, H. (2022). Theoretical study of the conduction band and energy gap of *GaInNAs/InP* quantum well structure. *Nanosystems, Nanomaterials, Nanotechnologies*, *20*(1), 15–23. https://doi.org/10.15407/nnn.20.01.015

Van, H. J., Mitterhuber, L., et al. (2023). Nanostructured Thermoelectric Films Synthesised by Spark Ablation and Their Oxidation Behaviour. *Nanofabrication and Nanomanufacturing*, *13*(11), 1778. https://doi.org/10.3390/nano13111778

Wang, F., Dong, A., et al. (2016). Solution–Liquid–Solid Synthesis, Properties, and Applications of One-Dimensional Colloidal Semiconductor Nanorods and Nanowires. *Chemical Reviews*, *116*(18), 10888–10933. https://doi.org/10.1021/acs.chemrev.5b00701

Yue, L.-Q., Shi, Y.-L., et al. (2023). InP Low-Dimensional Nanomaterials for Electronic and Optoelectronic Device Application. *Advanced Sensor Research*, *2*(10), 2200101. https://doi.org/10.1002/adsr.202200101

Zhang, J., Xu, W., et al. (2017). Organic Donor–Acceptor Complexes as novel organic semiconductors. *American Chemical Society*, *50*(7), 1654–1662. https://doi.org/10.1021/acs.accounts.7b00124

Zhang, Z., Fengm, C., et al. (2020). Electrochemical deposition as a universal route for fabricating single-atom catalysts. *Nature Communications*, *11*(1), 1215. https://doi.org/10.1038/s41467-020-14917-6